

NASA CR-173,367

NASA-CR-173367  
19840014932

# A Reproduced Copy

OF

NASA CR-173,367

**LIBRARY COPY**

AUG 5 0 1984

LANGLEY RESEARCH CENTER  
LIBRARY, NASA  
HAMPTON, VIRGINIA

Reproduced for NASA

*by the*

**NASA Scientific and Technical Information Facility**



NF01465



N84

230001

UNCLAS

D1

N84 23001

### Introduction

This is the fifth quarterly report on Contract NAS5-27382 entitled, "Spectroradiometric Calibration of the Thematic Mapper and the Multispectral Scanner System." In this report, we provide the results of an analysis that relates TM saturation level to ground reflectance, calendar date, latitude, and atmospheric condition. We also include a revised version of the preprint included with the last quarterly report for publication in the IEEE Transactions on Geoscience and Remote Sensing. The paper is entitled "In-flight Absolute Radiometric Calibration of the Thematic Mapper."

### Sensor Radiance for a Midlatitude Atmospheric Model

To account for all orders of multiple scattering, the Herman radiative transfer code iteratively traces solar radiance through a discrete number of scattering angles and many atmospheric layers. Because of the large amount of computing time required, this has proved to be rather costly. Recently, however, the code has been transferred from the University computer system to an IBM personal computer. It can now be run continuously on this dedicated system. Although our system is equipped with 512K bytes of memory, only 192K bytes are required to run the code. A portion of the additional memory is configured as a "superdrive" where programs, such as the Fortran 77 compiler, are stored. Thus, when the source code needs to be recompiled, the code is read from RAM memory, rather than from floppy disks. Compilation time

is reduced by a factor of four, to about 10 minutes. Currently we are awaiting the arrival of Digital's Fortran compiler (just released to dealers this week). This software will support complex arithmetic and also the 8087 math processor chip. It is believed that use of the 8087 will reduce the run time of the Herman code by an order of magnitude. This would allow an average calculation to be done in about 15 minutes.

The first data generated on the IBM are presented here. We wished to use the code to predict what ground reflectance would saturate the TM sensor output given a standard midlatitude atmospheric model. This model atmosphere is somewhat difficult to characterize due to the large variations in aerosol and water vapor levels. Although no single optical depth component can characterize aerosol scattering, measurements by Elterman<sup>1</sup> have allowed a rough correlation to be made between atmospheric visibility and the Mie optical depth,  $\tau_{Mie}$ . At a wavelength of 0.55  $\mu\text{m}$  and with extremely clear atmospheric conditions a typical value of  $\tau_{Mie}$  is 0.2. To bracket this aerosol level,  $\tau_{Mie}$  values at 0.55  $\mu\text{m}$  of 0.1 and 0.3 were also used as inputs. These three  $\tau_{Mie}$  values can be correlated with atmospheric conditions corresponding to 20 km, 40 km, and greater than 100 km visibility. When using such a correlation, one must keep in mind that it is an extrapolation based upon data taken between what was defined as 2 km and 13 km visibilities. For any of these atmospheres a range of spectral  $\tau_{Mie}$  values was computed using the relationship  $\tau_{Mie} = b\lambda^{-(\nu-2)}$ . This spectral dependence was found by assuming a Junge radial size distribution, with  $dN/dr = cr^{-(\nu+1)}$  and  $\nu = 2.5$ .

The ozone optical depth components were computed by using the U. S. Standard Atmosphere (USSA) Midlatitude Ozone Model value of 347 matm-cm for columnar ozone.<sup>2</sup> Using the spectral absorption coefficients of Vigroux,<sup>3</sup>  $\tau_{O_2}$  was computed for the wavelengths of interest. Absorption due to water vapor also had to be accounted for in band 4. The LOWTRAN V code was used to compute the transmittance of several lines within this band for the USSA water vapor content of 1.17 gm/cm<sup>2</sup>. These transmittances were averaged to compute a model  $\tau_{H_2O}$  value. Rayleigh scattering is accounted for by computing  $\tau_{Ray}$  using an atmospheric pressure of 1013 mb. Finally, the exo-atmospheric solar irradiance was accounted for by assuming the published values of Neckel and Labs,<sup>4</sup> given at an earth-sun distance of 1 AU. The values of these parameters are summarized in the tables to follow, as well as the code outputs.

The output of the Herman radiative transfer code gives the upwelling radiance that is leaving the atmosphere and incident at the entrance pupils of the Landsat 4 and 5 sensors. This radiance is compared to the radiance level at which saturation occurs. The latter value is known from the prelaunch calibration in which a 122-cm integrating sphere was used to determine the gains, offsets, and dynamic ranges for each channel and each band.<sup>5</sup> Later, reference was made to the on-board internal calibration system to monitor postlaunch changes. Knowing the gain (G) and offset (O) coefficients, the maximum allowed radiance value can be computed by setting the digital counts (C) to 255 in the calibration equation  $C = GL + O$ . This is the radiance which, when incident on the entrance pupil, would exceed 255 output digital counts

following the use of the Radiometric Look-Up Table (RLUT). The saturation radiance values, as used in the 15 JAN 84 update to the TIPS data processing system are:

BAND	1	2	3	4	5	7
$L_{sat}$ ( $mW/cm^2 \mu m sr$ )	15.21	29.68	20.43	20.62	2.719	1.438

Figures 1 through 4 plot the Herman code output as a function of solar zenith angle (from the data tabulated in Table 1). To utilize these figures, solar zenith angles at the time of Landsat overpass must be known. This is approximated in Figure 5, which gives these angles verses time of year and latitude.<sup>6</sup> The figure captions summarize the conditions required to saturate the various bands. Figure 6 shows that the ground reflectance corresponding to 255 digital output counts is relatively independent of aerosol loading. The last figure, Fig. 7, plots the radiance at the sensor for a ground reflectance of  $\rho = 0.75$  and solar zenith angle of  $45^\circ$ .

Band 1

$\lambda$	= 0.485	$\tau_{Mie}$	= 0.2130
$E_0$	= 190.81	$\tau_{Ray}$	= 0.1622
$L_{sat}$	= 15.21	$\tau_{ox}$	= 0.0100

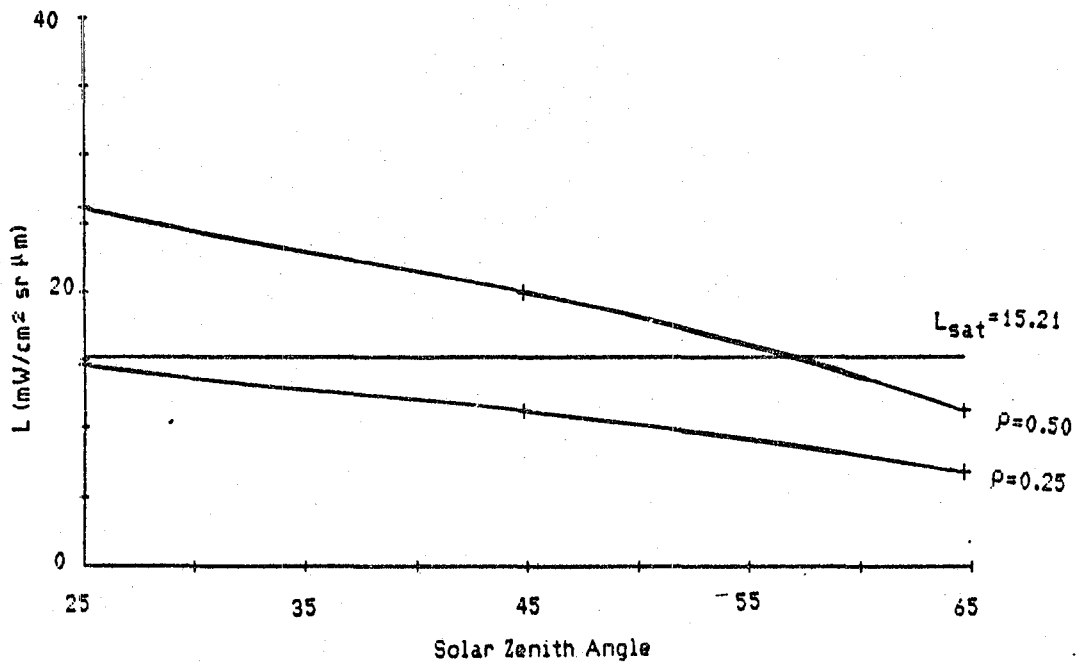


Fig. 1. Radiance at the sensor as a function of solar zenith angle for a visibility of 40 km. This shows, for example, that  $\rho=0.25$  does not give rise to saturation but  $\rho=0.50$  is only unsaturated from mid-September to mid-March at  $55^\circ\text{N}$ , from roughly mid-November to early February at  $30^\circ\text{N}$ , and remains saturated through the whole year for  $15^\circ\text{N}$  and  $0^\circ\text{N}$  latitudes.

Band 2

$\lambda$  = 0.57  
 $E_0$  = 180.34  
 $L_{sat}$  = 29.68

$\tau_{Mie}$  = 0.1965  
 $\tau_{Ray}$  = 0.0839  
 $\tau_{oz}$  = 0.0429

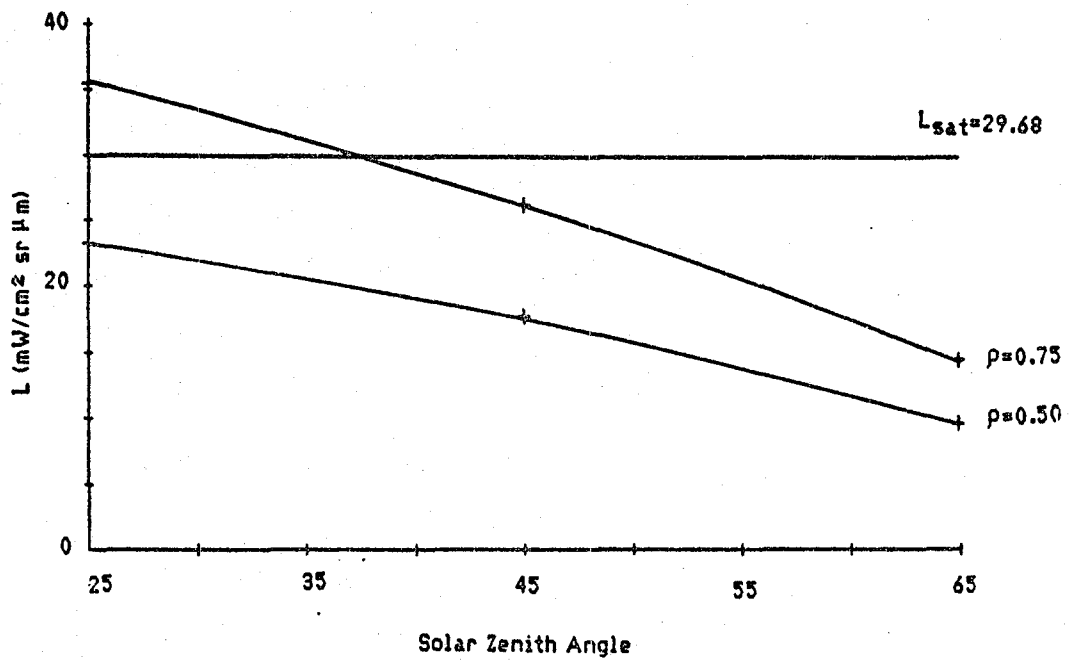


Fig. 2. Band 2 remains unsaturated throughout the year for ground reflectances less than  $\rho = 0.50$ . The  $\rho = 0.75$  curve crosses the saturation line at a solar zenith angle of about 38°. Thus the sensor will output less than 255 digital counts from mid-July to May at 55°N latitude, from September to April at 30°N, from late September to March at 15°N, and from October to March at 0°N.

ORIGINAL PAGE IS  
OF POOR QUALITY

7

Band 3

$\lambda$	= 0.66 $\mu\text{m}$	$\tau_{\text{Mie}}$	= 0.1826
$E_0$	= 150.66	$\tau_{\text{Ray}}$	= 0.0462
$L_{\text{sat}}$	= 20.43	$\tau_{\text{oz}}$	= 0.0215

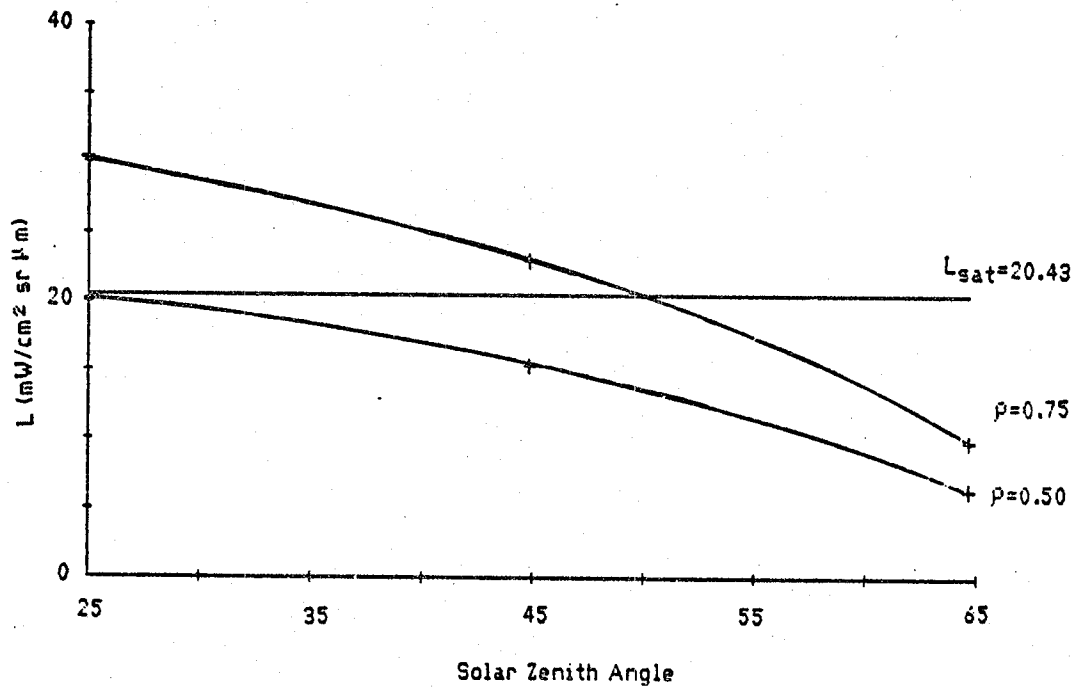


Fig. 3. In band 3 the sensor remains unsaturated for a ground reflectance of  $\rho = 0.50$  or less. At  $\rho = 0.75$  the sensor is unsaturated from about early September to April at  $55^\circ\text{N}$  latitude, from mid-October through late February at  $30^\circ\text{N}$ , and is saturated for lower latitudes for the entire year.

Band 4

$\lambda$	= 0.84	$\tau_{Mie}$	= 0.1618
$E_0$	= 104.19	$\tau_{Ray}$	= 0.0175
$L_{sat}$	= 20.62	$\tau_{oz}$	= 0.0024; $\tau_{H_2O}$ = 0.0700

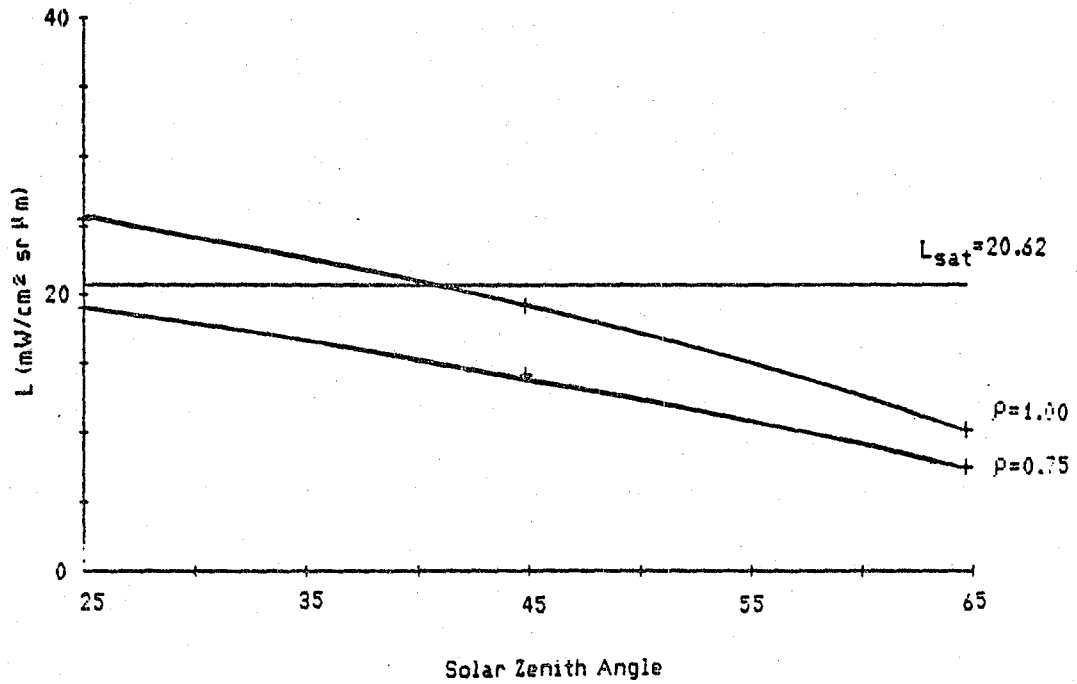


Fig. 4. Band 4 remains unsaturated for  $\rho=0.75$  or less. At a ground reflectance of  $\rho = 1.00$  the sensor is unsaturated from late July to mid-May at  $55^\circ\text{N}$ , from September to early April at  $30^\circ\text{N}$ , from early October to March at  $15^\circ\text{N}$ , and from early November to February at  $0^\circ\text{N}$ .

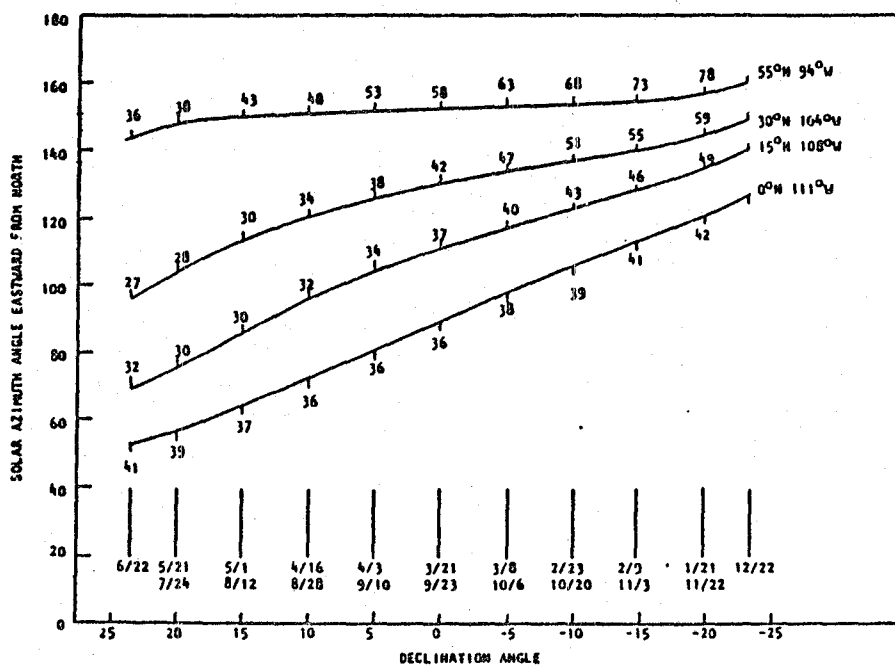


Fig. 5. Solar zenith angle as a function of time of year for four latitudes over a typical portion of the descending node of a Landsat orbit.

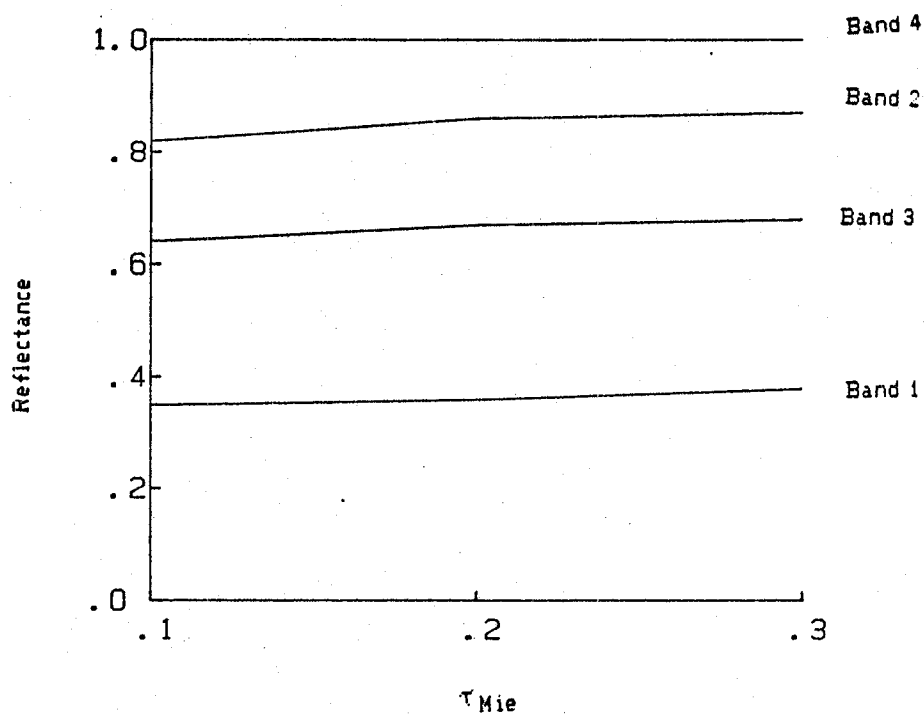
ORIGINAL PAGE IS  
OF POOR QUALITY

Fig. 6. Values of ground reflectance required to saturate the TM sensor for three different aerosol loading conditions (corresponding to about 20 km, 40 km, and greater than 100 km visibility) and a solar zenith angle of 45°. The  $\tau_{Mie}$  values are given for a wavelength of 0.55  $\mu\text{m}$ , and vary slightly from band to band.

CENTRE OF SCIENCE  
OF POOR QUALITY

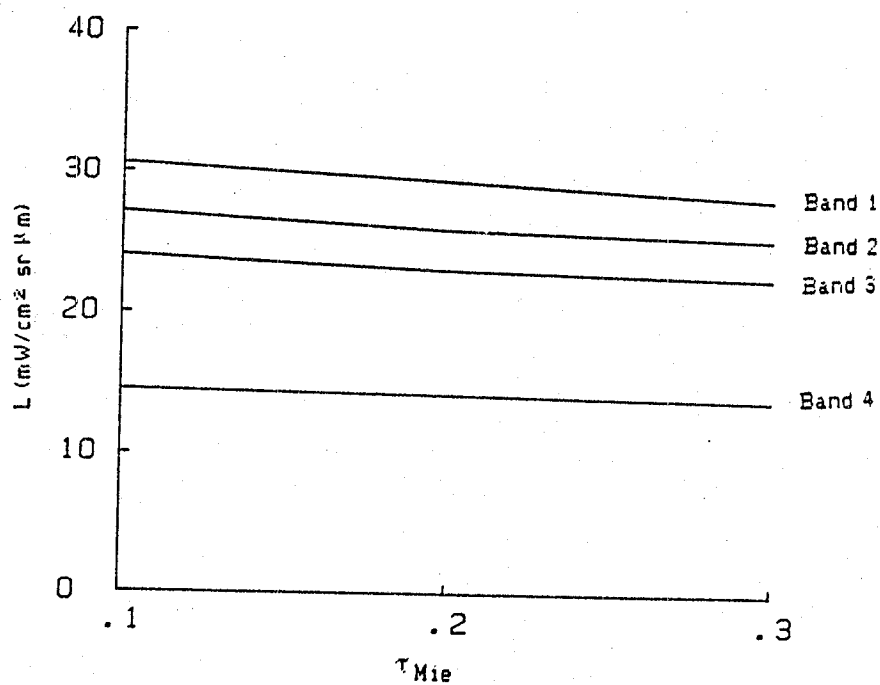


Fig. 7. Radiance  $L$  ( $\text{mW}/\text{cm}^2 \text{ sr } \mu\text{m}$ ) for the first 4 TM bands, given a ground reflectance of  $\rho = 0.75$  and solar zenith angle of  $\theta_z = 45^\circ$ . Values of  $\tau_{\text{Mie}}$  are for  $\lambda = 0.55 \mu\text{m}$  and correspond to 3 levels of aerosol content (visibility).

Table I. Output radiance  $L(\text{mW}/\text{cm}^2 \text{ sr } \mu\text{m})$  from Herman code.

Band 1				
$\tau_{\text{Mie}}$	$\theta_z$	L		
		$\rho = 0.25$	$\rho = 0.50$	$\rho_{\text{sat}}$
0.1065	25	14.82	27.06	0.26
	45	11.42	20.63	0.35
	65	6.89	11.85	0.67
0.2130	25	14.60	26.26	0.26
	45	11.38	19.92	0.36
	65	6.90	11.30	0.70
0.3195	25	14.36	25.36	0.27
	45	10.99	19.18	0.38
	65	6.62	10.75	0.74

Band 2				
$\tau_{\text{Mie}}$	$\theta_z$	L		
		$\rho = 0.50$	$\rho = 0.75$	$\rho_{\text{sat}}$
0.0982	25	24.02	35.76	0.62
	45	18.27	27.07	0.82
	65	10.24	14.96	----
0.1965	25	23.08	35.17	0.64
	45	17.65	25.91	0.86
	65	9.53	14.35	----
0.2947	25	22.65	33.99	0.66
	45	16.93	25.32	0.87
	65	9.20	-----	-----

**Band 3**

$\tau_{Mie}$	$0_z$	L		$\rho_{sat}$
		$\rho = 0.50$	$\rho = 0.75$	
0.0913	25	20.84	31.35	0.49
	45	15.97	24.00	0.64
	65	9.15	13.64	-----
0.1826	25	20.22	30.39	0.51
	45	15.34	23.02	0.67
	65	8.60	12.74	-----
0.2739	25	19.90	29.92	0.51
	45	15.01	22.51	0.68
	65	8.31	12.25	-----

**Band 4**

$\tau_{Mie}$	$0_z$	L		$\rho_{sat}$
		$\rho = 0.75$	$\rho = 1.00$	
0.0809	25	19.24	25.83	0.80
	45	14.52	19.49	-----
	65	7.89	10.56	-----
0.1618	25	18.98	25.57	0.81
	45	14.22	19.15	-----
	65	7.57	10.14	-----
0.2428	25	18.67	25.22	0.82
	45	13.89	18.74	-----
	65	7.25	9.73	-----

### References

1. L. Elterman, "Vertical-Attenuation Model With Eight Surface Meteorological Ranges 2 to 13 Kilometers." Air Force Cambridge Research Laboratories, AFCRL-70-0200, March 1970.
2. S. L. Valley, ed. "Handbook of Geophysics and Space Environments," McGraw-Hill, 1965.
3. E. Vigroux, "Contributions a l'etude experimentale de l'absorption de l'ozone." Ann. Phy. (Paris), 8, 709 (1953).
4. H. Neckel and D. Labs, "Improved data of solar spectral irradiance from 0.33 to 1.25  $\mu\text{m}$ ," Solar Phys. 74, 231 (1981)
5. J. Barker, NASA/GSFC, Greenbelt, MD. Private communication.
6. P. N. Slater and R. D. Jackson, "Atmospheric effects on radiation reflected from soil and vegetation as measured by orbital sensors using various scanning directions." Appl. Opt. 21, 3923 (1982).

N84

230002

UNCLAS

N84 23002

*D2*  
15

APPENDIX

**IN-FLIGHT ABSOLUTE RADIOMETRIC CALIBRATION OF THE THEMATIC MAPPER**

K. R. Castle, R. G. Holm, C. J. Kastner, J. M. Palmer, and P. N. Slater

Optical Sciences Center  
University of Arizona  
Tucson, AZ 85721, USA

M. Dinguirard

Centre d'Etudes et de Recherches de Toulouse  
2, Avenue Edouard-Belin  
31055 Toulouse, Cedex, France

C. E. Ezra and R. D. Jackson

Agricultural Research Service  
U.S. Department of Agriculture  
Phoenix, AZ 85040, USA

R. K. Savage

Atmospheric Sciences Laboratory  
White Sands Missile Range, NM 88002, USA

**ABSTRACT**

Ground spectral reflectance and atmospheric spectral optical depth measurements made at White Sands, New Mexico on January 3, 1983, were used with an atmospheric radiative transfer program to determine the spectral radiance at the entrance pupil of the Landsat-4 Thematic Mapper (TM). A comparison with the output digital counts of the TM, when imaging the measured ground area, provided an absolute calibration for five detectors in TM bands 2, 3, and 4. By reference to an adjacent, larger

uniform area, the calibration was extended to all 16 detectors in each of the three bands. Pre-flight calibration results agreed with these in-flight measurements to 6.6%, 2.4%, and 12.9% in bands 2, 3, and 4 respectively.

#### I. INTRODUCTION

The Thematic Mapper (TM) multispectral scanner system was placed into earth orbit on July 16, 1982, as part of NASA's Landsat-4 payload. The entire system had been calibrated in an absolute sense at Santa Barbara Research Center before launch (1, 2). During flight, an internal calibration system monitors the calibration of the focal plane (3). To determine temporal changes of the absolute radiometric calibration of the entire system in flight, we initiated a program at White Sands, New Mexico, on January 3, 1983, to make spectroradiometric measurements of the ground and the atmosphere simultaneously with TM image acquisitions over that area (4). By entering our measured values into an atmospheric radiative transfer program (5), we determined the radiance levels at the entrance pupil of the TM in four of the TM spectral bands (full width at half maximum: band 1, 0.45-0.52  $\mu\text{m}$ ; band 2, 0.53-0.61  $\mu\text{m}$ ; band 3, 0.62-0.69  $\mu\text{m}$ ; and band 4, 0.78-0.91  $\mu\text{m}$ ). These levels were compared to the output digital counts from the detectors that sampled the radiometrically measured ground area, thus providing an absolute radiometric calibration of the entire TM system utilizing those detectors. Then, by reference to an adjacent, larger uniform area, the calibration was extended to all 16 detectors in each of the three bands.

## II. DETERMINATION OF SPECTRAL RADIANCE AT THE TM FROM SITE MEASUREMENTS

On January 3, 1983, an 80-mm layer of two-day-old snow covered the flat gypsum surface at the White Sands Missile Range. The reflectance of the snow was measured by reference to a 1.2 x 1.2-m barium sulfate panel using a Barnes Modular Multispectral 8-Channel Radiometer (Model 12-1000) (6), which collected radiant flux simultaneously in all the TM spectral bands over a total field angle of 15°. The instrument was mounted on a rotatable boom 2.5 m above the snow to allow an average radiance value to be determined for an area of about 0.5 x 5 m. The measurements were made at 1708 GMT, coinciding with the overpass of the TM. The solar zenith angle was 62.8°. With the radiance of the barium sulfate panel at 62.8° as a reference, the reflectance of the snow in TM bands 1 to 4 was found to be 0.769, 0.761, 0.756, and 0.732 respectively, with an rms uncertainty of ±0.02 in all cases.

After the TM overpass, hand-held Exotech (6) radiometer measurements were made at the pixel centers of a 4 x 4 pixel area on the snow (pixel size 30 x 30 m) to check for significant differences from the Barnes radiometer data. Variations between the Barnes and the Exotech data were small and attributed to variations introduced by the Exotech measurement technique rather than in the snow reflectance. The 4 x 4 pixel area was later found to be at an angle to the scan lines; as a result, the individual detectors obtained different numbers of samples (see Table 6).

By reference to an access road and nearby frozen water surfaces we were able to accurately locate the known reflectance area on the TM imagery.

A solar radiometer (7) using nine 10-nm-wide spectral bands in the visible and near ir was used to determine the total spectral optical depths  $\tau'_{ext}$  at these nine wavelengths. The measured barometric pressure of 889.5 mbar allowed the Rayleigh spectral optical depth  $\tau'_{Ray}$  to be determined. From these data the Mie and ozone spectral optical depths (8) were determined.

In bands TM 1, 2, and 3, the component of  $\tau'_{ext}$  due to molecular absorption,  $\tau'_{abs}$ , is due entirely to ozone. In band 4, water vapor and  $CO_2$  predominate. Their effects have been included in Table 1, which lists the values for the various atmospheric constituents in bands 1 through 4.

Because of the limitations of the instruments used on January 3,  $\tau'_{abs}$  in band 4 due to water vapor and  $CO_2$  could not be measured. Instead, the LOWTRAN code (9) was used to compute the water vapor and  $CO_2$  transmittances across band 4 at  $5\text{ cm}^{-1}$  intervals. The water vapor transmittance was scaled, to account for the 44% relative humidity measured at White Sands on January 3, then averaged to find  $\tau'_{H_2O+CO_2}$ . The effect of an error in this estimate can be judged by noting that the inclusion of water vapor and  $CO_2$  lowered the predicted radiance level at the TM by only 2%.

TABLE 1. ATMOSPHERIC VALUES.

<u>Band</u>	<u><math>\lambda_c</math> (<math>\mu\text{m}</math>)</u>	<u><math>\tau'_{\text{ext}}</math></u>	<u><math>\tau'_{\text{Mie}}</math></u>	<u><math>\tau'_{\text{Ray}}</math></u>	<u><math>\tau'_{\text{abs}}</math></u>
1	0.485	0.291	0.148	0.142	0.001
2	0.57	0.218	0.138	0.074	0.006
3	0.66	0.172	0.128	0.041	0.003
4	0.84	0.134	0.110	0.015	0.009

The data in Table 1 and the reflectance values quoted above were used as inputs to the Herman and Browning (5) radiative transfer code. In using the code, the atmosphere is divided into a sufficient number of plane-parallel layers such that changes in radiance within each layer are due only to single scattering processes. The Gauss-Seidel iterative technique is used to solve the equation of radiative transfer. Upon convergence, all multiple scattering effects have been taken into account. A Junge radial size distribution was assumed for the aerosols. A  $\nu$  value of 2.5 was assumed in the equation for radial distribution:

$$\frac{dN}{dr} = Cr^{-(\nu+1)} \quad (1)$$

where  $r$  is the aerosol radius. Values of 5.02  $\mu\text{m}$ , 0.02  $\mu\text{m}$ , and 0.04  $\mu\text{m}$  were used for the maximum and minimum radii and incremental step size, respectively, for the aerosols. The aerosols were given a refractive index of 1.54-0.01  $i$  and assumed to have a vertical distribution as measured by Elterman (10).

The following quantities were calculated by the code. Their values are listed in Table 2.

- $E_{D,Dir}$ : The downward direct solar irradiance at the ground is  $E_0 \cos \theta_z \exp(-\tau'_{ext} \sec \theta_z)$  where  $E_0$  is the exoatmospheric solar irradiance and  $\theta_z$  is the solar zenith angle
- $E_{D,Dif}$ : The downward diffuse solar irradiance at the ground
- $L_{U,Dir}$ : The upward direct radiance at the TM due to  $E_{D,Dir}$  and  $E_{D,Dif}$ .
- $L_{U,P}$ : The upward path radiance at the TM is
- $$L_T - (E_{D,Dir} + E_{D,Dif}) \frac{\rho}{\pi} \exp(-\tau'_{ext} \sec 5^\circ)$$
- $L_T$ : The total radiance at the TM at a  $5^\circ$  nadir angle.

TABLE 2. IRRADIANCES AND RADIANCES (NORMALIZED TO UNITY SOLAR EXOATMOSPHERIC IRRADIANCE).

BAND	SOLAR ZENITH	$\frac{E_{D,Dir}}{E_0}$	$\frac{E_{D,Dif}}{E_0}$	$\frac{L_{U,Dir}}{E_0}$	$\frac{L_{U,P}}{E_0}$	$\frac{L_T}{E_0}$
	ANGLE					
1	55°	0.345	0.185	0.097	0.033	0.130
	65°	0.212	0.152	0.067	0.025	0.092
2	55°	0.392	0.145	0.105	0.024	0.129
	65°	0.253	0.122	0.073	0.019	0.092
3	55°	0.425	0.122	0.111	0.019	0.130
	65°	0.282	0.104	0.078	0.015	0.093
4	55°	0.454	0.095	0.112	0.014	0.126
	65°	0.308	0.082	0.079	0.011	0.090

Values for the exoatmospheric irradiances within the TM passbands,  $E_0$ , were found by evaluating

$$E_0 = \frac{1}{d^2} \int_{\lambda_1}^{\lambda_2} E_{0\lambda} d\lambda \quad (2)$$

where  $d = 0.983$  astronomical units for January 3,  $\lambda_1$  and  $\lambda_2$  are the wavelength limits of the TM passbands as determined by using the equivalent passband technique of Palmer and Tomasko (11), and  $E_{0\lambda}$  is the exoatmospheric solar spectral irradiance data of Neckel and Labs (12). The integration was carried out using 2 to 10-nm intervals as dictated by the resolution of the Neckel and Labs data. The required values of  $L_T/E_0$  for the center wavelength of each band and the solar zenith angle of  $62.8^\circ$  were found by interpolating between the  $55^\circ$  and  $65^\circ$  radiative transfer code data in Table 2. These, when multiplied by their corresponding  $E_0$  values, gave the radiances in  $\text{mWcm}^{-2}\text{sr}^{-1}$  in the TM passbands listed in Table 3. (An error of less than 1% is introduced using the value at the center wavelength of each band instead of evaluating

$$E_0 = \frac{1}{d^2} \int_{\lambda_1}^{\lambda_2} E_{0\lambda} \cdot l(\lambda) d\lambda,$$

where  $l(\lambda)$  is the output as a function of wavelength from the radiative transfer code, as given by  $L_T/E_0$  in Table 2.)

**TABLE 3. EXOATMOSPHERIC IRRADIANCES AND THE RADIANCES AT THE TM IN THE TM PASSBANDS AS DETERMINED FROM SITE MEASUREMENTS AT WHITE SANDS.**

<u>BAND</u>	<u>EQUIVALENT TM BANDWIDTH in <math>\mu\text{m}</math></u>	<u>WAVELENGTH LIMITS IN <math>\mu\text{m}</math></u>	<u><math>E_0</math> in <math>\text{mWcm}^{-2}</math></u>	<u><math>L_T</math> in <math>\text{mWcm}^{-2}\text{sr}^{-1}</math></u>
1	0.0715	0.4503-0.5218	14.4	1.45
2	0.0887	0.5269-0.6156	16.6	1.66
3	0.0771	0.6213-0.6984	12.3	1.25
4	0.1349	0.7719-0.9068	14.7	1.44

**III. DETERMINATION OF AVERAGE IN-BAND RADIANCE AT THE TM FROM IMAGE DIGITAL COUNTS AND SYSTEM CALIBRATION DATA.**

We next describe how we determined corresponding sets of  $L_T$  values from pre-flight and in-flight internal calibration data. By identifying our site on the raw image data, we determined which detectors scanned the area and in what order, and how many samples each collected. The site was scanned from north to south by detector numbers 3, 2, 1, 16, and 15, in that order. They collected 1, 3, 5, 4, and 2 samples respectively. We found the average digital count for each detector, using offset and gain values reported by Barker et al. (1), then calculated the average spectral radiance,  $L_T$ , from  $L_T = (\text{average count} - \text{offset}) / \text{gain}$ . (Throughout this paper, spectral radiances are referred to the entrance pupil). These spectral radiances were multiplied by the number of samples for each detector. The resultant products were added and then divided by

the total number of samples, 15. Thus we derived a value for the average spectral radiance of our site as measured by the TM, proportionally weighted according to the number of samples per detector. These values are listed in Table 4.

TABLE 4. AVERAGE COUNTS AND SPECTRAL RADIANCES (in  $\text{mWcm}^{-2}\text{sr}^{-1}\mu\text{m}^{-1}$ ) FOR FIVE DETECTORS IN TM BANDS 2, 3 AND 4 AS CALCULATED FROM PRE-FLIGHT CALIBRATION DATA (1).

DETECTOR	BAND 2		BAND 3		BAND 4	
	AVERAGE COUNT	AVERAGE SPECTRAL RADIANCE	AVERAGE COUNT	AVERAGE SPECTRAL RADIANCE	AVERAGE COUNT	AVERAGE SPECTRAL RADIANCE
3	139.0	17.04	165.0	15.40	133.0	11.89
2	143.7	17.42	169.7	15.86	132.0	12.02
1	146.2	17.52	171.6	15.73	134.2	12.00
16	141.5	17.43	167.8	15.85	132.0	12.01
15	147.5	17.65	172.5	15.88	131.5	12.05
<b>WEIGHTED AVERAGE</b>		17.46		15.78		12.01

Then the average spectral radiance per band was multiplied by the equivalent bandwidth to provide the weighted average radiance in each band. (These values are listed in column B of Table 5.)

Barker et al. (2) have reported that the TM internal calibrator, used in flight, indicates that the response of TM bands 1 through 4 has slowly decreased with time during the period July-December 1982. We have used the Barker et al. data to change the pre-launch calibration

data. The changed values are listed in column C of Table 5. With respect to this decrease in response, we note, first, that the internal calibrator compares the response of only the TM filters, detectors, and electronics to seven different irradiance levels; it does not measure any change in transmittance of the image-forming system. Second, it is possible that the decrease in response is wholly or partly due to a change in the output of the internal calibrator.

Table 5 summarizes our results based on measurements at White Sands and compares them to pre-flight calibration and in-flight calibration data from the TM internal calibrator.

TABLE 5. COMPARISON OF RADIANCES ( $\text{mWcm}^{-2}\text{sr}^{-1}$ ) IN TM BANDS 2, 3 AND 4.

BAND	COLUMN A	COLUMN B	COLUMN C	$(\frac{A-B}{A})\%$	$(\frac{A-C}{A})\%$
2	1.66	1.55	1.50	6.6	9.8
3	1.25	1.22	1.16	2.4	7.2
4	1.44	1.62	1.57	-12.9	-9.6

COLUMN A GIVES THE RADIANCE LEVELS AT THE TM AS DERIVED FROM GROUND AND ATMOSPHERIC MEASUREMENTS AT WHITE SANDS ON JANUARY 3, 1983, AND THE USE OF AN ATMOSPHERIC RADIATIVE TRANSFER PROGRAM (SEE TABLE 3).

COLUMN B GIVES THE WEIGHTED AVERAGE RADIANCE IN EACH PASSBAND ( $\text{mWcm}^{-2}\text{sr}^{-1}$ ) AS DETERMINED FROM TM IMAGE DATA OF OUR WHITE SANDS SITE IN CONJUNCTION WITH PRE-FLIGHT CALIBRATION DATA.

COLUMN C GIVES THE VALUES IN COLUMN B AS MODIFIED BY THE CHANGE IN RESPONSE SUGGESTED BY THE INTERNAL CALIBRATOR DATA OF DECEMBER 8, 1982.

Because of the small number of samples collected over the test site and the small variation in the digital counts recorded by each detector in each band, the most meaningful way to summarize the results of the calibration is to list the individual counts for each detector and the radiance in each band. This has been done in Table 6. Note that whereas there are significant detector-to-detector variations within a band, the variations for a given detector are consistent with the expected uncertainty in the output of the analog-to-digital converter for a constant input analog signal.

**TABLE 6. DIGITAL COUNTS FOR EACH DETECTOR THAT SAMPLED THE GROUND SITE AND THE RADIANCE AT THE TM DETERMINED FROM THE MEASUREMENTS AT WHITE SANDS.**

DETECTOR NUMBER:						RADIANCE AT TM, ( $\text{mWcm}^{-2}\text{sr}^{-1}$ )
	3	2	1	16	15	
BAND 2	139	143	147	141	147	1.66
		144	146	141	148	
		143	145	141		
			147	143		
			146			
BAND 3	165	170	172	167	172	1.25
		169	172	167	172	
		170	171	168		
			171	169		
			172			
BAND 4	133	132	134	133	130	1.44
		131	134	131	133	
		133	134	131		
			134	133		
			135			

#### IV. EXTENSION OF CALIBRATION TO OTHER DETECTORS

To extend the calibration of the five detectors in each band to all 16 detectors in each band, a  $10 \times 16$  pixel test site of uniform reflectance was selected from an analysis of the TM imagery of White

Sands. This site was 500 m southwest of the  $4 \times 4$  pixel test site described earlier. Its uniformity was such that none of the 16 rows of 10 pixels exhibited a variance of greater than 1.5 digital counts, the average variance being 0.9 digital count. The average number of digital counts for each of the 16 detectors in each band in this  $10 \times 16$  pixel area is listed in Table 7. To verify, a posteriori, that the large site had the same reflectance as the  $4 \times 4$  pixel site, the digital counts were compared for detectors 3, 2, 1, 16, and 15 in the three bands. For the 15 detectors that sampled both sites (five each in three bands) the digital count difference between the two sites was less than 1 for nine of the detectors.

It is interesting to note that there was no evidence of a level shift, as described by Kleffer et al. (14), in this part of the scene. The  $10 \times 16$  pixel area was selected on the basis of its close statistical match to the  $4 \times 4$  pixel area and was later found to have been scanned by detectors 1 through 8 in one direction and by detectors 9 through 16 in the reverse direction. However, in other parts of the scene, certain detectors did exhibit a level shift of up to 3 counts.

The average digital count values in Table 7 can be compared to our computed TM entrance pupil radiance values given in Column A of Table 5 to provide a single point calibration for all detectors in TM bands 2, 3, and 4.

**TABLE 7. AVERAGE DIGITAL COUNTS FOR THE 10 × 16 PIXEL TEST SITE IN THE THREE TM BANDS.**

<u>DETECTOR</u>	<u>BAND 2</u>	<u>BAND 3</u>	<u>BAND 4</u>
1	145.4	171.5	133.8
2	142.7	167.8	131.0
3	141.0	167.4	133.0
4	143.0	166.8	131.4
5	145.2	168.4	131.2
6	144.0	168.7	132.4
7	142.8	167.3	131.7
8	142.5	167.5	132.0
9	143.4	168.8	132.6
10	142.1	167.5	137.2
11	141.4	166.3	130.9
12	141.7	169.8	132.7
13	145.2	168.6	134.2
14	143.8	168.9	132.3
15	146.2	170.2	130.7
16	141.0	167.1	132.1

#### V. UNCERTAINTIES IN THE CALIBRATION PROCEDURE

There are four sources of uncertainty in the calibration procedure. These have been discussed elsewhere (4) and will be only briefly referred to here.

The main uncertainty is in our knowledge of the composition, size distribution, and vertical distribution of atmospheric aerosols. Of these, the value assumed for the aerosol complex index is the most critical. On the basis of a survey of aerosol conditions at White Sands by Jennings et al. (15), we estimated that an error of ±3.5% is introduced if extreme rather than the assumed average conditions existed on the morning of the calibration measurements. Departures of aerosol size and vertical

distributions from the assumed average can give rise to a  $\pm 2\%$  change in radiance at the TM. We thus have a root-sum-of-the-squares (rss) uncertainty of  $\pm 4\%$  due to an imprecise knowledge of atmospheric conditions.

An uncertainty of  $\pm 2\%$  is attributed to the combination of three reflectance-related factors: nonuniformities in the ground reflectance, uncertainty in the knowledge of the absolute reflectance of the reference panel, and the departure of the ground and reference surfaces from being Lambertian reflectors.

An uncertainty of  $\pm 1\%$  is due to the uncertainty in the exoatmospheric spectral irradiance data of Neckel and Labs (11).

An uncertainty of  $\pm 0.7\%$  is due to a variation of  $\pm 1$  digital count in an output of 150 counts from the TM in the imaging of a constant radiance level.

If we assume an error of  $\pm 2\%$  due to the neglect of polarization effects, the overall rss uncertainty in the calibration procedure is  $\pm 5\%$ .

Henceforth, to reduce the uncertainty to less than  $\pm 3\%$ , we plan to take the following steps:

1. Collect aircraft spectropolarimeter data, calibrated in an absolute sense, to check the calibration procedure and determine the magnitude of any possible systematic errors.
2. Collect aircraft imagery of the ground reference areas to accurately map spatial variations in ground reflectance.

3. Make ground measurements simultaneously with TM overpasses at sites having different reflectances.
4. Use a version of the Herman and Browning atmospheric radiative transfer program (5) that accounts for polarization and the nonlambertian characteristics of the ground surfaces.
5. Attempt to more precisely estimate the aerosol composition and distributions by:
  - a. Making ground level diffuse and direct irradiance measurements.
  - b. Applying inversion techniques.
  - c. Making more detailed atmospheric measurements, e.g. of the Babinet and Arago points.

## VI. CONCLUSIONS

The absolute calibration of five detectors in TM bands 2, 3, and 4, as determined by measurements at White Sands on January 3, 1983, is given in Table 6. Pre-flight calibration results agree with these in-flight measurements to 6.6%, 2.4% and 12.9% in bands 2, 3, and 4 respectively. Table 7 shows the absolute calibration extended to all the detectors in bands 2, 3, and 4. The estimated uncertainty in these results is  $\pm 5\%$ ; the estimated uncertainty in the pre-flight calibration is no better than  $\pm 6\%$  (1, 16).

Band 1 saturated over the snowfield at White Sands. Pre-flight data (1) indicate that a saturation level of 255 counts corresponds to a radiance at the sensor of  $1.14 \text{ mWcm}^{-2}\text{sr}^{-1}$  in TM band 1. We estimate that the snowfield provided a radiance level of  $1.45 \text{ mWcm}^{-2}\text{sr}^{-1}$  at the sensor.

We are presently fabricating field equipment to provide more detailed and accurate measurements of the surface and atmosphere at White Sands. Our goal is to reduce the uncertainty in sensor absolute calibration to less than  $\pm 3\%$ .

We plan to continue the work described here to include the in-flight absolute radiometric calibration of the Landsat-5 Multispectral Scanner System and TM and the Systeme Probatoire d'Observation de la Terre, Haute Résolution Visible (SPOT/HRV) systems.

#### VII. ACKNOWLEDGMENTS

We wish to thank B. M. Herman for the use of his radiative transfer code, J. A. Reagan for the use of his solar radiometer, and both for useful discussions. We would like to thank B. L. Markham for pointing out an inconsistency in an early draft of the paper. The University of Arizona authors wish to acknowledge support from NASA (contract number NAS5-27382), J. L. Barker, Science Representative and the USDA (broadform contract number 12-14-5001-38).

## REFERENCES

1. J. L. Barker, D. L. Ball, K. C. Leung, and J. A. Walker, "Prelaunch absolute radiometric calibration of the reflective bands on the Landsat-4 protoflight thematic mapper." Proceedings of the Landsat-4 Early Results Symposium, NASA Goddard Space Flight Center, in press (1983).
2. J. L. Barker, R. B. Abrams, D. L. Ball, and K. C. Leung, "Characterization of radiometric calibration of Landsat-4 TM reflective bands." Proceedings of the Landsat-4 Early Results Symposium. NASA Goddard Space Flight Center, in press (1983).
3. P. N. Slater, "A review of radiometric calibration problems." Proc. Int'l Coll., Spectral Signatures of Objects in Remote Sensing, Bordeaux, France. In press (1983).
4. C. J. Kastner and P. N. Slater, "In-flight radiometric calibration of advanced remote sensing systems." Proc. SPIE Symposium, Field Measurement and Calibration Using Electro-Optical Equipment: Issues and Requirements 356, pp. 158-165 (1982).
5. B. M. Herman and S. R. Browning, "The effect of aerosols on the earth-atmosphere albedo." J. Atmos. Sci., 32, 1430 (1975).
6. Trade names and company names are included for the benefit of the reader and do not constitute an endorsement by the Centre d'Etudes et de Recherches de Toulouse, the University of Arizona, the United States Army, Atmospheric Sciences Laboratory, or the United States Department of Agriculture.
7. G. E. Shaw, J. A. Reagan, and B. M. Herman, "Investigations of atmospheric extinction using direct solar radiation measurements made with a multiple wavelength radiometer." J. Appl. Meteorol., 12, 374 (1973).
8. M. D. King and D. M. Byrne, "A method for inferring total ozone content from the spectral variation of total optical depth obtained with a solar radiometer." J. Atmos. Sci., 33, 2242-2251 (1976).
9. F. X. Kneizys, E. P. Shettle, W. O. Gallery, J. H. Chetwynd, Jr., L. W. Abreu, J. E. A. Selby, R. W. Fenn, and R. A. McClatchey. "Atmospheric transmittance/radiance: computer code LOWTRAN 5." AFGL-TR-80-0067 (February 1980).
10. L. Elterman, "Aerosol measurements in the troposphere and stratosphere," Appl. Opt., 5, 1769 (1966).

11. J. M. Palmer and M. G. Tomasko, "Broadband radiometry with spectrally selective detectors." *Optics Letters*, 5, 208-210 (1980).
12. E. Neckel, and D. Labs, "Improved data of solar spectral irradiance from 0.33 to 1.25  $\mu\text{m}$ ." *Solar Phys.* 74, 231 (1981).
13. J. L. Barker, NASA Goddard S.F.C., personal communication that included spectral responsivities of TM bands in digital form as measured at Santa Barbara Research Center (1983).
14. H. H. Kieffer, E. M. Eliason and P. S. Chavez Jr., "Thematic mapper intraband radiometric performance." *Proceedings of the Landsat-4 Early Results Symposium, NASA Goddard Space Flight Center, in press (1983).*
15. S. G. Jennings, R. G. Pinnick, and H. J. Auvermann, "Effects of particulate complex refractive index and particle size distribution variations on atmospheric extinction and absorption for visible through middle ir wavelengths." *Appl. Opt.*, 17 3922 (1978).
16. V. T. Norwood, and J. C. Lansing, Jr., "Electro-optical imaging sensors." Chapter 8 in *Manual of Remote Sensing*, 2nd ed., ed. R. N. Colwell, p. 367, American Society of Photogrammetry, Falls Church, Virginia (1983).

**End of Document**